New Results from the Spectral Observations of Solar Coronal Type II Radio Bursts

R. Ramesh[1] , C. Kathiravan[1], and S. Surya Natarajan[2]
[1] Indian Institute of Astrophysics, Koramangala 2nd Block, Bangalore, Karnataka, 560034, India
[2] Delft University of Technology, Mekelweg, 2628 Delft, The Netherlands

Abstract

We carried out a statistical study of twenty-six type II radio bursts from the Sun observed with the Gauribidanur Low-frequency Solar Spectrograph in the frequency range 85–35 MHz during the period 2009–2019. Our results indicate that the average instantaneous bandwidth of the type II bursts in the above frequency range correlates with the angular width of the associated coronal mass ejections (CMEs). The correlation coefficient is ≈71%. This independently indicates that the coronal type II bursts reported in this work are mostly due to shocks driven by the CMEs. Moreover, it also suggests that the instantaneous bandwidth of the bursts could be due to electron acceleration (leading to type II bursts) occurring simultaneously at multiple locations of differing electron densities (i.e., plasma frequencies) along the shock surrounding the CME.

Unified Astronomy Thesaurus concepts: The Sun (1693); Solar coronal mass ejections (31); Solar radio emission (1522); Radio bursts (1339)

1. Introduction

Type II radio bursts from the Sun appear on spectrograph records as intense, narrow bands of transient emission drifting toward lower frequencies. The drift rate decreases with decreasing frequency. The bursts result from the excitation of plasma waves in the ambient medium due to nonthermal electrons accelerated by a shock propagating outwards through the solar atmosphere. It is generally accepted that the radio waves are emitted near the local electron plasma frequency (f_p) and/or its harmonics. The corresponding emissions in the spectra are called the fundamental (F) and harmonic (H) components of the type II burst. Sometimes, either or both of the F and H bands of emission are split into two bands or branches, the lower frequency branch (LFB) and the upper frequency branch (UFB). Such events are called split-band type II bursts. At times, type II bursts exhibit multiple separate lanes that are different from the classical band-splitting mentioned above (see, e.g., Nelson & Melrose 1985 for details). The drift of the bursts from high to low frequencies is due to the decrease of the electron density (N_e) in the solar atmosphere with increasing heliocentric distance (r). The aforesaid shocks accelerate solar energetic particles (SEPs) and produce sudden storm commencement (SSC) events at Earth also. Both solar flares and coronal mass ejections (CMEs) are capable of giving rise to large-amplitude magnetohydro-dynamic (MHD) waves in the solar atmosphere. If the speed of the latter exceeds the local Alfvén speed (v_A), then a shock is formed. The electrons accelerated by the shock result in type II bursts. While it is widely accepted that the type II radio bursts observed in the outer corona and the interplanetary medium are due to the CMEs (see, e.g., Sheeley et al. 1985; Vršnak & Cliver 2008), the energetic disturbance responsible for the shocks that generate the type II bursts observed in the near-Sun corona is still being debated. Note that the former events are collectively called the interplanetary type II bursts and are observed over the frequency range corresponding to decameter −hectometer and kilometer wavelengths. The near-Sun events are called the coronal type II bursts and are observed over frequencies corresponding to meter wavelengths. Several studies indicate that CMEs are responsible for the coronal type II bursts, too (see, e.g., Aurass 1997; Cliver et al. 1999; Maia et al. 2000; Lara et al. 2003; Cho et al. 2005; Gopalswamy 2006; Lin et al. 2006; Subramanian & Ebenezer 2006; Shanmugaraju et al. 2006; Cho et al. 2008; Gopalswamy et al. 2009; Ramesh et al. 2010b, 2012a; Gopalswamy et al. 2013; Kouloumvakos et al. 2014; Zucca et al. 2014a, 2014b; Hariharan et al. 2015; Kumari et al. 2017a, 2019), but flares and various other eruptive activity have also been reported as drivers of the shocks that generate these bursts (see, e.g., Klassen et al. 1999; Vršnak 2001; Nindos et al. 2008; Pick & Vilmer 2008; Magdalenić et al. 2010; Nindos et al. 2011; Alissandrakis et al. 2021). Therefore, any result that independently constrains the shock driver of the near-Sun type II bursts would be useful and important. In this connection we wanted to compare the instantaneous bandwidth of the coronal type II bursts (Mann et al. 1995; Cunha-Silva et al. 2015) and the angular width of the associated CMEs. To our knowledge, such a study is rare among the published reports of statistical analyses involving large data sets of CMEs and coronal type II bursts (see, e.g., Claßen & Aurass 2002; Shanmugaraju et al. 2003; Gopalswamy et al. 2005; Shanmugaraju et al. 2006). Hence the present work.

2. Observations

The radio spectral data were obtained with the Gauribidanur LOw-frequency Solar Spectrograph (GLOSS) in the frequency range 85–35 MHz (Ebenezer et al. 2001, 2007; Kishore et al. 2014; Hariharan et al. 2016b). The GLOSS is operated by the Indian Institute of Astrophysics (IIA) at the Gauribidanur Observatory (Ramesh 2011; Ramesh et al. 2014) located about 100 km north of Bangalore. It is a one-dimensional array of eight log-periodic dipole antennas (LPDAs; Ramesh et al. 1998) set up along a North−South baseline. The half-power width of the response pattern of GLOSS for observations near
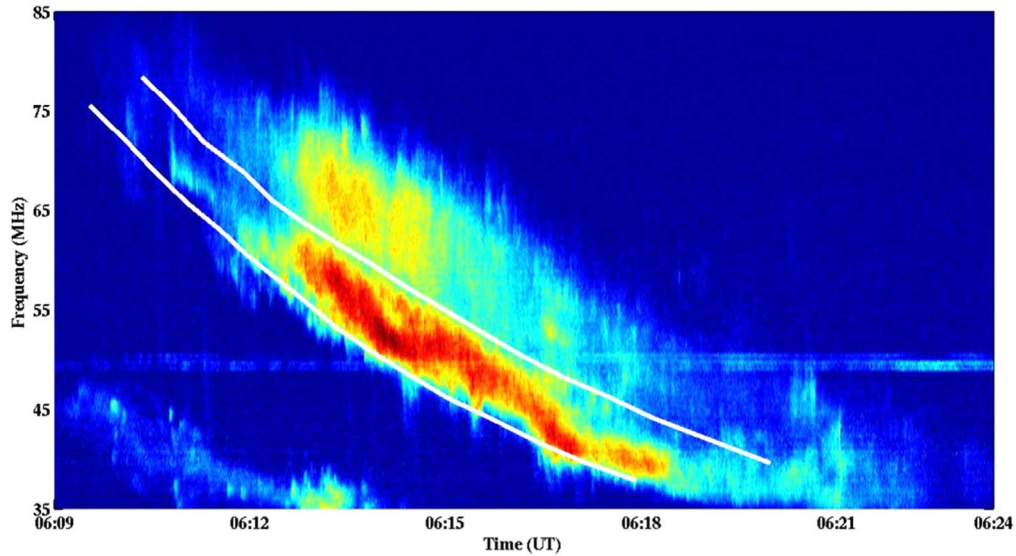
Figure 1. GLOSS dynamic spectrum of the F-H SB type II solar radio burst observed on 2014 December 5. The horizontal patch of emission near $\approx$50 MHz is an artifact and is due to local radio frequency interference (RFI). The two "slanted" white lines marked on the type II burst are the quadratic least-squares fits to the instantaneous lower and upper frequency limits of the LFB of the H component of the burst. The F component of the burst could be partly noticed near the lower left corner of the spectra. It is also comparatively fainter.

the zenith is $\approx$90° $\times$ 6° (R.A. $\times$ decl.) at the highest frequency of operation, i.e., 85 MHz. While the width of the response pattern along R.A. is nearly independent of frequency, its width along the declination varies inversely with the frequency. The observations were carried out with an integration time of $\approx$1 s and a bandwidth of $\approx$1 MHz. The minimum detectable flux density is $\approx$75 Jy (1 Jy $= 10^{-26}$ W m^{-2} Hz^{-1}) at a typical frequency such as 80 MHz. The antenna and the receiver systems were calibrated by carrying out observations in the direction of the Galactic Center as described in Kishore et al. (2015). We also used data obtained with the Gauribidanur RAdio Spectro-Polarimeter (GRASP; Sasikumar Raja et al. 2013a; Hariharan et al. 2015; Kishore et al. 2015; Mugundhan et al. 2018), e-CALLISTO (Monstein et al. 2007; Benz et al. 2009), and the Kodaikanal Solar Observatory Radio Spectrograph (KRS; Indrajit et al. 2021) to supplement GLOSS observations. For information on the CMEs, we used the catalog generated from observations with the Large Angle and Spectrometric Coronagraph C2 (LASCO-C2; Brueckner et al. 1995) on board the Solar and Heliospheric Observatory (SOHO).[3]

3. Results

Figure 1 shows the dynamic spectrum of the split-band type II burst observed with the GLOSS on 2014 December 5. The burst had both F and H components. The burst was associated with a C1.8 class (peak flux $\approx 1.8 \times 10^{-6}$ W m^{-2}) GOES soft X-ray flare reported in the interval $\approx$05:57–06:17 UT with a maximum at $\approx$06:07 UT.[4] The SOHO/LASCO-C2 coronagraph observed a CME at $\approx$06:24 UT when the leading edge (LE) of the latter was at $r \approx 2.8\,R_\odot$. The extrapolation of the CME height–time (h–t) data indicates that the CME LE was close to $r \approx 2\,R_\odot$ during the appearance of the type II burst at 80 MHz around $\approx$06:10 UT. The central position angle (CPA, measured counterclockwise from the solar north) of the

CME is $\approx$304°. Its angular width is $\approx$172°, and the linear speed in the plane of sky (POS) is $\approx$534 km s^{-1}. The mass and kinetic energy of the CME are $\approx 6.3 \times 10^{15}$ g and $\approx 9 \times 10^{30}$ erg, respectively. We used a quadratic least-squares fit to the instantaneous upper and lower frequency limits of the LFB of the H component of the split-band burst (see Figure 1), and estimated its average bandwidth in the frequency range 85–35 MHz. Similar details for all of the type II bursts and CMEs used in the present work are listed in Table 1.

The radio data set consists of different known categories of type II bursts: simple events with a single lane (SL), complex bursts with multiple lanes (ML), and those with split-band (SB) structure in their respective dynamic spectra. The source regions of the CMEs were identified from the locations of the associated Hα activity. They were located chiefly in the equatorial belt of the Sun, i.e., the 30°S–30°N heliographic latitude range, except for the event of 2013 November 9 (S.No. 14 in Table 1), whose source region was located at 70°S latitude. Regarding their heliographic longitudes, it is a combination of events located near the disk center ($<$20°), mid-longitudes (20°–70°), and close to the limb ($>$70°). The bursts tabulated were specifically chosen because they were clearly noticeable in the observations and hence their bandwidths could be determined unambiguously (see, e.g., Aguilar-Rodriguez et al. 2005). The average bandwidth for the events listed in Table 1 is $\approx$7 MHz (see Column 5). This is consistent with the typical bandwidths of $\approx$4 MHz in the $\approx$50–35 MHz range (Carley et al. 2021), and $\approx$2–3 MHz in the $\approx$30–10 MHz range (Melnik et al. 2004). Note that the instantaneous bandwidth of the type II bursts decreases with decreases in frequency (Aguilar-Rodriguez et al. 2005). We also calculated the relative instantaneous bandwidth (i.e., by dividing the instantaneous bandwidth by the mid-frequency of the corresponding band) for all of the events as mentioned in Aguilar-Rodriguez et al. (2005). The values are in the range 0.10–0.29 (see Column 5 in Table 1). These are reasonably consistent with the average value of 0.23 $\pm$ 0.13 reported by the above authors.

3 https://cdaw.gsfc.nasa.gov/CME_list/
4 https://ftp.swpc.noaa.gov/pub/warehouse/

Table 1
Details Related to the Type II Bursts Observed with GLOSS during the Period 2009–2019 and the Associated SOHO/LASCO-C2 CMEs

S. No.	Date	Burst Interval (UT)	Burst type	Bandwidth / Relative Bandwidth (MHz/-)	CME Width (deg)	Single CME	Active Region Location
1	2009 Dec 22	04:57–05:05	SL(F-H)	7.4/0.19	47	Yes	S26W46
2	2010 Jun 13	05:39–05:56	SB(F-H)	6.3/0.29	33	No	S25W84
3	2011 May 21	07:42–07:55	SL(F-H)	7.5/0.19	38	Yes	···
4	2011 Aug 2	06:08–06:28	ML	6.7/0.15	268	Yes	N14W15
5	2011 Sep 20	07:01–07:12	SL	4.9/0.12	54	Yes	N21E58
6	2011 Oct 1	09:07–09:22	SL(F-H)	6.5/0.16	203	Yes	N10W06
7	2011 Nov 17	07:27–07:32	SB	6.8/0.10	97	Yes	S19E08
8	2012 Mar 9	03:42–04:11	SL(F-H)	12.4/0.28	360	Yes	N15W01
9	2012 Mar 24	08:50–08:55	SB	5.5/0.12	105	Yes	S25E80
10	2012 Apr 30	07:26–07:41	SL	5.3/0.11	135	Yes	S22E62
11	2012 Aug 3	06:03–06:18	SL(F-H)	6.5/0.13	74	Yes	S22E55
12	2013 May 2	05:05–05:22	SB(F-H)	6.3/0.16	99	Yes	N10W26
13	2013 Oct 25	02:59–03:14	SB(F-H)	5.6/0.14	121	Yes	S10E75
14	2013 Nov 19	10:26–10:41	SB	8.8/0.15	360	Yes	S70W14
15	2013 Dec 12	03:18–03:35	SL	9.6/0.16	276	Yes	S23W46
16	2014 Jan 8	03:52–04:02	SB(F-H)	4.4/0.11	108	Yes	N11W81
17	2014 Feb 11	03:30–03:47	ML	4.9/0.11	81	No	S12E17
18	2014 Apr 19	09:25–09:33	SL	6.5/0.12	32	Yes	···
19	2014 Jul 25	07:12–07:20	ML	4.9/0.11	79	Yes	N09E35
20	2014 Aug 14	04:02–04:10	SB(F-H)	5.5/0.14	27	Yes	S20W63
21	2014 Aug 22	10:28–10:42	ML	9.9/0.25	360	Yes	N12E01
22	2014 Nov 6	03:43–03:51	SL	5.1/0.10	210	Yes	N17E58
23	2014 Dec 5	06:09–06:25	SB(F-H)	7.6/0.19	172	Yes	S21W69
24	2015 Aug 28	06:29–06:46	ML	5.1/0.13	86	Yes	S14W63
25	2015 Oct 17	04:21–04:27	ML	5.3/0.11	70	Yes	S15E75
26	2015 Nov 4	03:26–03:41	ML	6.5/0.14	64	Yes	N15W64

Note. SL—Single lane; SB—Split band; ML—Multiple lane.

While majority of the bursts are due to fundamental (F) plasma frequency emission, a few of them are due to harmonic (H) emission. The F component in the case of the latter was below the lower frequency limit (i.e., 35 MHz) of GLOSS, as in Figure 1. Having said so, it should be noted that the widths of the F and H emission bands in the type II bursts are nearly the same (Mann et al. 1995, 1996). In the case of the bursts that exhibited SB emission features (see Figure 1), we considered the LFB of the burst because the corresponding emission is from the corona ahead of the shock, i.e., the upstream region (Smerd et al. 1974; Vršnak et al. 2001; Zimovets et al. 2012; Hariharan et al. 2014; Cunha-Silva et al. 2015; Kishore et al. 2016; Kumari et al. 2017b; Chrysaphi et al. 2018), similar to the type II bursts without SB features. Some of the type II bursts listed in Table 1 have multiple lanes. We used the bandwidth of the lowermost frequency lane for the analysis in such events, too. The drift rate of the different lanes in each event was nearly the same as in the SB events. Moving on to the observations on 2010 June 13 and 2014 February 11 (S. Nos. 2 and 17 in Table 1, respectively), we found that in both the cases there were two spatially close CMEs with a potential association to the type II burst. But we could rule out one CME in each case, since their extrapolated speeds in the near-Sun corona during the type II burst period were comparatively smaller ($<$200 km s^{-1}).

4. Analysis

Using the data in Table 1, we estimated the correlation between the average instantaneous bandwidth of the type II bursts and the angular width of the associated CMEs. The results are shown in Figure 2. There is a significant correlation between the bandwidth of the type II bursts and the angular width of the associated CMEs. We would like to add here that both of the above quantities are directly measurable from the respective observations (i.e., radio and white light) without any assumptions. This indicates that the type II bursts listed in Table 1 are likely due to shocks driven by the associated CMEs.

The different locations from the nose to the flanks of the shock will be at different heliocentric distances (see, e.g., Mancuso & Raymond 2004; Gopalswamy et al. 2012; Kumari et al. 2019; Frassati et al. 2019; Morosan et al. 2019). This implies that N_e and hence f_p at the respective locations will be different (Alissandrakis et al. 2021). Recently, Jebaraj et al. (2021) and Kouloumvakos et al. (2021) showed that type II radio emission occurs at locations where the shock is supercritical with a quasi-perpendicular geometry. These conditions can be unique to different parts of the shock. Note that a shock is said to be quasi-perpendicular if the angle between the shock normal and the upstream magnetic field is $>$45°. The critical Alfvén Mach number (M_A^c) for such a shock is typically in the range $\approx$1.1–2.8 depending on the local plasma parameters (Benz & Thejappa 1988; Mann et al. 1995). According to Edmiston & Kennel (1984), M_A^c is very sensitive and is between 1 and 2 for typical solar wind parameters. Shocks whose Alfvén Mach number (M_A) exceeds M_A^c corresponding to that particular location are said to be supercritical. It was noted by Vršnak & Cliver (2008) that coronal type II burst shocks propagate generally at $M_A \lesssim 2$. Zucca et al. (2018) presented evidence for coronal type II
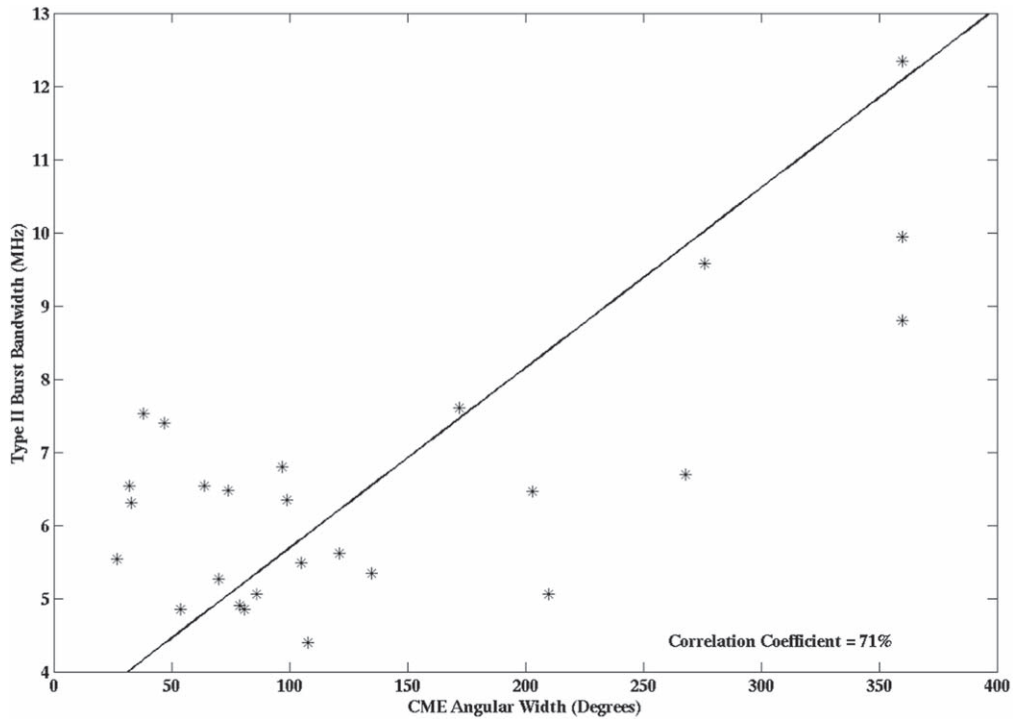
Figure 2. Bandwidth of the type II bursts observed with the GLOSS during the period 2009–2019 in the frequency range 85–35 MHz vs. the angular width of the associated CMEs. The straight line is the linear least-squares fit to the data points.

emission from a region with a quasi-perpendicular shock geometry and Mach number in the range $\approx$1.3–1.5 based on model calculations and observations. Reports indicate that the shock geometry in the low corona could be quasi-perpendicular at several regions on the shock (see, e.g., Gopalswamy et al. 2012; Maguire et al. 2020; Carley et al. 2021). According to Mann et al. (1995), subcritical quasi-perpendicular shocks could generate coronal type II bursts. Assuming that all of the aforementioned conditions are favorable for the generation of type II emission, it is very likely that they would be satisfied at multiple locations or along an extended region on the shock.

Knock et al. (2003) reported modeling of type II burst dynamic spectra assuming a parabola-shaped global shock that had multiple electron acceleration regions with a quasi-perpendicular geometry. In a following paper, Knock & Cairns (2005) showed that CMEs with a larger lateral extent give rise to type II emission with broader bandwidths. The wider CMEs have wider shocks and a larger area where the electrons gain energy via shock acceleration (Michalek et al. 2007). CMEs/ shocks with a smaller radius of curvature are expected to be radio quiet (Cairns et al. 2003) without any accompanying nonthermal radio bursts (see, e.g., Kathiravan et al. 2002; Ramesh et al. 2021). Multifrequency radio imaging data show that the centroids of the type II bursts observed at different frequencies at the same time are laterally displaced (see, e.g., Gary et al. 1984; Zimovets & Sadykov 2015; Zucca et al. 2018; Morosan et al. 2019; Kouloumvakos et al. 2021). This suggests the cotemporal occurrence of type II radio bursts from an extended region with different N_e and hence f_p values on the shock ahead of a CME (see, e.g., McLean 1967). The correlation between the average instantaneous bandwidths of the type II bursts and the angular widths of the associated CMEs in the present case (see Figure 2) is consistent with the aforementioned model calculations and observations.

5. Summary

We analyzed twenty-six low-frequency (85–35 MHz) type II solar radio bursts observed with the GLOSS during the period 2009–2019, along with the associated CMEs and flares. It is found that the average instantaneous bandwidth of the bursts correlates well with the angular width of the CMEs. The correlation coefficient is $\approx$71%. This indicates that: (1) the coronal type II bursts reported in the present work are most likely due to shocks driven by the CMEs, and (2) the acceleration of electrons leading to the bursts occurs simultaneously at multiple locations or over an extended region on the shock, which in turn has a bearing on the instantaneous bandwidth of the bursts. Spectral observations with better temporal and spectral resolutions (see, e.g., Mugundhan et al. 2017; Carley et al. 2021) might improve the above correlation since any possible overestimation of the burst bandwidth in events where SB and/or multilane features are present would be minimal. White-light observations over $r \lesssim 2\ R_\odot$ (for example, with the soon to be launched Visible Emission Line Coronagraph on board the ADITYA-L1, the first Indian space solar mission; Singh et al. 2011) where the coronal type II radio bursts generally occur would be also helpful. However, it must be noted that a wider CME need not always imply a correspondingly larger instantaneous bandwidth for the type II burst, since other factors such as frequency blocking (Knock et al. 2003), variations of the upstream plasma parameters and the local shock normal across the macroscopic shock, etc. (Knock & Cairns 2005; Schmidt & Cairns 2016) also play a role.

ORCID iDs

R. Ramesh   https://orcid.org/0000-0003-2651-0204

References

Aguilar-Rodriguez, E., Gopalswamy, N., MacDowall, R., Yashiro, S., & Kaiser, M. L. 2005, JGR, 110, A12S08

Alissandrakis, C. E., Nindos, A., Patsourakos, S., & Hillaris, A. 2021, A&A, 654, A112

Aurass, H. 1997, in Coronal Physics from Radio and Space Observations, ed. G. Trottet, Vol. 483 (Berlin: Springer), 135

Benz, A. O., Monstein, C., Meyer, H., et al. 2009, EM&P, 104, 277

Benz, A. O., & Thejappa, G. 1988, A&A, 202, 267

Brueckner, G. E., Howard, R. A., Koomen, M. J., et al. 1995, SoPh, 162, 357

Cairns, I. H., Knock, S. A., Robinson, P. A., & Kuncic, Z. 2003, SSRv, 107, 27

Carley, E. P., Cecconi, B., Reid, H. A., et al. 2021, ApJ, 921, 3

Cho, K.-S., Bong, S.-C., Kim, Y.-H., Moon, Y.-J., et al. 2008, A&A, 491, 873

Cho, K.-S., Moon, Y.-J., Dryer, M., et al. 2005, JGRA, 110, A12101

Chrysaphi, N., Kontar, E. P., Holman, G. D., & Temmer, M. 2018, ApJ, 868, 79

Claßen, H. T., & Aurass, H. 2002, A&A, 384, 1098

Cliver, E. W., Webb, D. F., & Howard, R. A. 1999, SoPh, 187, 89

Cunha-Silva, R. D., Fernandes, F. C. R., & Selhorst, C. L. 2015, A&A, 578, A38

Ebenezer, E., Ramesh, R., Subramanian, K. R., Sundara Rajan, M. S., & Sastry, C. V. 2001, A&A, 367, 1112

Ebenezer, E., Subramanian, K. R., Ramesh, R., Sundara Rajan, M. S., & Kathiravan, C. 2007, BASI, 35, 111

Edmiston, J. P., & Kennel, C. F. 1984, JPlPh, 32, 429

Frassati, F., Susino, R., Mancuso, S., & Bemporad, A. 2019, ApJ, 871, 212

Gary, D. E., Dulk, G. A., House, L., et al. 1984, A&A, 134, 222

Gopalswamy, N. 2006, in Solar Eruptions and Energetic Particles, ed. N. Gopalswamy, R. Mewaldt, & J. Torsti, Vol. 165 (New York: Wiley), 207

Gopalswamy, N., Aguilar-Rodriguez, E., Yashiro, S., et al. 2005, JGRA, 110, A12S07

Gopalswamy, N., Nitta, N., Akiyama, S., Mäkelä, P., & Yashiro, S. 2012, ApJ, 744, 72

Gopalswamy, N., Thompson, W. T., Davila, J. M., et al. 2009, SoPh, 259, 227

Gopalswamy, N., Xie, H., Mäkelä, P., Yashiro, S., & Akiyama, S. 2013, AdSpR, 51, 1981

Hariharan, K., Ramesh, R., & Kathiravan, C. 2015, SoPh, 290, 2479

Hariharan, K., Ramesh, R., Kathiravan, C., Abhilash, H. N., & Rajalingam, M. 2016, ApJS, 222, 21

Hariharan, K., Ramesh, R., Kishore, P., Kathiravan, C., & Gopalswamy, N. 2014, ApJ, 795, 14

Indrajit, V. B., Kathiravan, C., Gireesh, G. V. S., et al. 2021, SoPh, 296, 132

Jebaraj, I. C., Kouloumvakos, A., Magdalenić, J., et al. 2021, A&A, 654, A64

Kathiravan, C., Ramesh, R., & Subramanian, K. R. 2002, ApJL, 567, L93

Kishore, P., Kathiravan, C., Ramesh, R., Rajalingam, M., & Indrajit, V. B. 2014, SoPh, 289, 3995

Kishore, P., Ramesh, R., Hariharan, K., Kathiravan, C., & Gopalswamy, N. 2016, ApJ, 832, 59

Kishore, P., Ramesh, R., Kathiravan, C., & Rajalingam, M. 2015, SoPh, 290, 2409

Klassen, A., Aurass, H., Klein, K.-L., Hofmann, A., & Mann, G. 1999, A&A, 343, 287

Knock, S. A., & Cairns, I. H. 2005, JGRA, 110, A01101

Knock, S. A., Cairns, I. H., & Robinson, P. A. 2003, JGRA, 108, 1361

Kouloumvakos, A., Patsourakos, S., Hillaris, A., et al. 2014, SoPh, 289, 2123

Kouloumvakos, A., Rouillard, A., Warmuth, A., et al. 2021, ApJ, 913, 99

Kumari, A., Ramesh, R., Kathiravan, C., & Gopalswamy, N. 2017a, ApJ, 843, 10

Kumari, A., Ramesh, R., Kathiravan, C., & Wang, T. J. 2017b, SoPh, 292, 161

Kumari, A., Ramesh, R., Kathiravan, C., Wang, T. J., & Gopalswamy, N. 2019, ApJ, 881, 24

Lara, A., Gopalswamy, N., Nunes, S., Muñoz, G., & Yashiro, S. 2003, GeoRL, 30, 8016

Lin, J., Mancuso, S., & Vourlidas, A. 2006, ApJ, 649, 1110

Magdalenić, J., Marqué, C., Zhukov, A. N., Vršnak, B., & Žic, T. 2010, ApJ, 718, 266

Maguire, C. A., Carley, E. P., McCauley, J., & Gallagher, P. T. 2020, A&A, 633, A56

Maia, D., Pick, M., Vourlidas, A., & Howard, R. 2000, ApJL, 528, L49

Mancuso, S., & Raymond, J. C. 2004, A&A, 413, 363

Mann, G., Classen, T., & Aurass, H. 1995, A&A, 295, 775

Mann, G., Klassen, A., Classen, H.-T., et al. 1996, A&AS, 119, 489

McLean, D. J. 1967, PASA, 1, 47

Melnik, V. N., Konovalenko, A. A., Rucker, H. O., et al. 2004, SoPh, 222, 151

Michalek, G., Gopalswamy, N., & Xie, H. 2007, SoPh, 246, 409

Monstein, C., Ramesh, R., & Kathiravan, C. 2007, BASI, 35, 473

Morosan, D. E., Carley, E. P., Hayes, L. A., et al. 2019, NatAs, 3, 452

Mugundhan, V., Hariharan, K., & Ramesh, R. 2017, SoPh, 292, 155

Mugundhan, V., Ramesh, R., Kathiravan, C., Gireesh, G. V. S., & Hegde, A. 2018, SoPh, 293, 41

Nelson, G. J., & Melrose, D. B. 1985, in Solar Radiophysics: Studies of Emission from the Sun at Metre Wavelengths, ed. D. J. McLean & N. R. Labrum (Cambridge: Cambridge Univ. Press), 333

Nindos, A., Alissandrakis, C. E., Hillaris, A., & Preka-Papadema, P. 2011, A&A, 531, A31

Nindos, A., Aurass, H., Klein, K.-L., & Trottet, G. 2008, SoPh, 253, 3

Pick, M., & Vilmer, N. 2008, A&ARv, 16, 1

Ramesh, R. 2011, in ASI Conf. Ser. 2, 1st Asia-Pacific Solar Physics Meeting, ed. A. R. Choudhuri & D. Banerjee (Bengaluru: BASI), 55

Ramesh, R., Anna Lakshmi, M., Kathiravan, C., Gopalswamy, N., & Umapathy, S. 2012a, ApJ, 752, 107

Ramesh, R., Kathiravan, C., Sreeja, S. K., & Gopalswamy, N. 2010b, ApJ, 712, 188

Ramesh, R., Kathiravan, C., Sundara Rajan, M. S., Indrajit, V. B., & Rajalingam, M. 2014, in ASI Conf. Ser. 13, The Metrewavelength Sky, ed. J. N. Chengalur & Y. Gupta (Bengaluru: BASI), 19

Ramesh, R., Kumari, A., Kathiravan, C., Ketaki, D., & Wang, T. J. 2021, GeoRL, 48, e91048

Ramesh, R., Subramanian, K. R., Sundara Rajan, M. S., & Sastry, C. V. 1998, SoPh, 181, 439

Sasikumar Raja, K., Kathiravan, C., Ramesh, R., Rajalingam, M., & Indrajit, V. B. 2013, ApJS, 207, 2

Schmidt, J. M., & Cairns, I. H. 2016, in AIP Conf. Proc. 1720, Solar Wind (Melville, NY: AIP), 040014

Shanmugaraju, A., Moon, Y.-J., Cho, K.-S., Dryer, M., & Umapathy, S. 2006, SoPh, 233, 117

Shanmugaraju, A., Moon, Y.-J., Dryer, M., & Umapathy, S. 2003, SoPh, 215, 161

Sheeley, N. R., Jr., Howard, R. A., Michels, D. J., et al. 1985, JGR, 90, 163

Singh, J., Raghavendra Prasad, B., Venkatakrishnan, P., et al. 2011, CSci, 100, 167

Smerd, S. F., Sheridan, K. V., & Stewart, R. T. 1974, in IAU Symp. 57, Coronal Disturbances, ed. G. A. Newkirk (Dordrecht: Reidel), 389

Subramanian, K. R., & Ebenezer, E. 2006, A&A, 451, 683

Vršnak, B. 2001, JGR, 106, 25291

Vršnak, B., Aurass, H., Magdalenić, J., & Gopalswamy, N. 2001, A&A, 377, 321

Vršnak, B., & Cliver, E. W. 2008, SoPh, 253, 215

Zimovets, I., Vilmer, N., Chian, A. C.-L., Sharykin, I., & Struminsky, A. 2012, A&A, 547, A6

Zimovets, I. V., & Sadykov, V. M. 2015, AdSpR, 56, 2811

Zucca, P., Carley, E. P., Bloomfield, D. S., & Gallagher, P. T. 2014a, A&A, 564, A47

Zucca, P., Morosan, D. E., Rouillard, A. P., et al. 2018, A&A, 615, A89

Zucca, P., Pick, M., Demoulin, P., et al. 2014b, ApJ, 795, 68